AIAA JOURNAL
Vol. 31, No. 7, July 1993

Influence of Stator-Rotor Gap on Axial-Turbine Unsteady Forcing Functions

Theodosios Korakianitis*
Washington University, St. Louis, Missouri 63130

This paper investigates the effects of stator-to-rotor axial gap on the two-dimensional propagation of pressure disturbances due to potential-flow interaction between the blade rows and viscous-wake effects from upstream blade rows in axial-turbine-blade rotor cascades. Results are obtained by modeling the effects of the upstream stator viscous wake and potential-flowfield on the downstream rotor flowfield, and computing the unsteady flowfields in the rotor frame. The amplitudes of the two types of disturbances for typical turbines are based on a review of available experimental and computational data. The potential-flowfield is modeled as a sinusoidal pressure disturbance of amplitude 4% of the local pressure across the stator trailing edges that decays downstream. This potential-flow disturbance from upstream is affected by the potential-flowfield of the downstream cascade. The velocity wake is modeled as a Gaussian velocity defect of varying amplitude and width, depending on the stator-rotor gap between the blade rows. The wake amplitudes and widths are based on conservation of loss of incoming momentum to the rotor due to the wake. The axial gap between rotor and stator is varied to show how the two disturbances propagating in different directions reinforce or counteract each other at different stator-rotor gaps. The corresponding forces on rotor blades are computed for typical values of reduced frequency. Analyses of this type will enable turbomachinery designers to predict (and with geometric design modifications to reduce) the unsteady stresses acting on turbomachinery blades.

Nomenclature

a	= acoustic velocity [Eq. (4)]
B	= amplitude of potential variation [Eq. (6)]
b	= axial chord of rotor or stator cascade (lengths nondimensionalized with b_{rb})
C_L	= tangential loading (lift) coefficient
c	= local absolute-flow velocity [Eq. (3)]
c_n	= stator-outlet absolute-flow averaged velocity
c_x	= axial component of velocity
c_0	= rotor-inlet total sonic velocity [Eq. (11)]
D	= wake amplitude, fraction of c_n [Eq. (3)]
d	= stator-rotor axial gap (Fig. 1)
F,F'	= force and nondimensional force [Eq. (11)]
j	$\equiv \sqrt{-1}$ [Eq. (6)]
M,M_x,M_y	= Mach number and its components
M'_z	= moment (in the z direction) [Eq. (11)]
N	= number of blades [Eq. (1)]
R	$\equiv N_{rb}/N_{sb}$ stator-to-rotor-pitch ratio
S	= pitch of a cascade
t	= time (nondimensionalized by y/S_{sb})
u	= velocity component in the x direction
V	= component of velocity
v	= velocity component in the y direction
W	= characteristic wake width, fraction of S_{sb} [Eq. (3)]
(x,y,z)	= Cartesian coordinates
α	= flow angle
α_n	= angle of wake propagation at inlet, along c_n
Δ, δ	= perturbation operators (on p, u, and v)
$\Delta\epsilon$, ϵ	= angles locating the potential [Eqs. (8) and (10)]
ξ	= complex parameter for the x decay of Φ [Eq. (6)]
ρ	= relative total density at rotor inlet
Φ	= velocity potential defined by [Eq. (5)]
ω	= rotor passing frequency [Eq. (2)]
$\tilde{\omega}$	= reduced frequency parameter [Eq. (2)]

Subscripts

i,o	= cascade inlet, outlet respectively
ip	= flow property for potential-flow model
iw	= flow property in the wake
q	= suction (s) or pressure (p) side [Eq. (3)]
rb,sb	= rotor and stator blade row respectively
te	= location of upstream-cascade trailing edge
(x,y,z)	= components in cartesian coordinates
ϕ	= perturbation value due to potential [Eq. (5)]

Introduction

IN axial turbomachinery design, after the stator and rotor velocity diagrams and tangential loading (and therefore cascade velocity levels) are chosen, two important parameters dominating unsteady stator-rotor interactions are the reduced frequency and the stator-to-rotor-pitch ratio R. R is defined by

$$R \equiv \frac{N_{rb}}{N_{sb}} = \frac{S_{sb}}{S_{rb}} \tag{1}$$

and it is inversely proportional to the reduced frequency parameter defined by

$$\tilde{\omega} \equiv \frac{\omega \cdot b_{rb}}{c_x} = \frac{2\pi V_{rb} b_{rb}}{S_{rb} c_x} \cdot \frac{1}{R} \tag{2}$$

The sources of two-dimensional flow unsteadiness between the rotor and the stator are viscous velocity wakes shed from the trailing edge of the stator, inviscid potential-flow variations in time because of the relative motion of the lifting surfaces, two-dimensional vortices shed at the stator trailing edge, flutter of both cascades, and the effect of flow changes due to cooling flows in high-pressure high-temperature turbine stages.

Presented in part at the Sixth International Symposium on Unsteady Aerodynamics, Aeroacoustics and Aeroelasticity of Turbomachines and Propellers, Notre Dame, IN, Sept. 15–19, 1991; received Nov. 21, 1991; revision received Oct. 5, 1992; accepted for publication Oct. 13, 1992.

*Assistant Professor, Department of Mechanical Engineering, Campus Box 1185, One Brookings Drive. Member AIAA.

In Fig. 1 the velocity wakes are illustrated by the dotted regions starting at the stator trailing edges. (All lengths in this paper are nondimensionalized with the rotor axial chord b_{rb}). The potential-flow disturbance from the stator is illustrated as higher and lower regions of pressure (and potential), with maxima at the stator trailing edges (shown with lines bulging downstream) and with minima between the stator trailing edges (shown with lines bulging upstream). This potential-flowfield will be affected by the potential-flowfield of the downstream cascade. The potential-flow disturbance from the upstream row is shown to gradually decay downstream, while the wakes diffuse and spread downstream. The stators are shown dashed in the figure because the approach models the stator-disturbance/rotor interaction and not the full stator-rotor interaction.

As R increases, the stator potential-flow disturbance relative to the rotor increases, and its frequency and decay rate decrease. For a fixed rotor geometry, as R increases, the physical size of the stator increases, and therefore one may observe a modest change in the amplitude and width of the wake (because of the longer lengths over which the boundary layers develop on the larger stators). In Fig. 1 $R = 52/31 = 1.67742$, which is close enough to $R = 5/3 = 1.666\ldots$ to make the wake centerlines every three stators (shown with stripes) to appear touching the leading edge of every five rotors (shown black) on both sides of the figure. On the left side, the axial gap is $d = 0.4$. A local minimum in potential enters the passage below the black rotor, and a local maximum in potential enters the passage above the black rotor. On the right side, the axial gap is $d = 0.8$. The relative "phase" of the disturbances has changed, and a local maximum in potential enters the passage below the black rotor, and a local minimum in potential enters the passage above the black rotor. This figure illustrates that by varying the axial gap between blade rows one expects to alter the relative locations of influence of the potential and wake disturbances in the downstream cascade. Similarly, the relative size of the two disturbances is affected by the stator-to-rotor-pitch ratio. The choice of R in Fig. 1 is arbitrary and for illustration purposes only, but in a region where both wake and potential-flow disturbances are important in the rotor flowfield, as will be explained below.

For the remainder of this paper we define as wakes the velocity defects generated by the surface boundary layers of upstream blade rows and propagating downstream. Because there is no static pressure jump at the trailing edge of blades, the wakes by this definition do not include a static pressure variation at the trailing edges where they are generated. We also define as potential-flow interaction the static pressure variation generated by the existence of the lifting surfaces and by the relative motion between the cascades. Static pressure perturbations due to potential-flow interaction are observed both upstream and downstream of the blade-surface region that generates it.

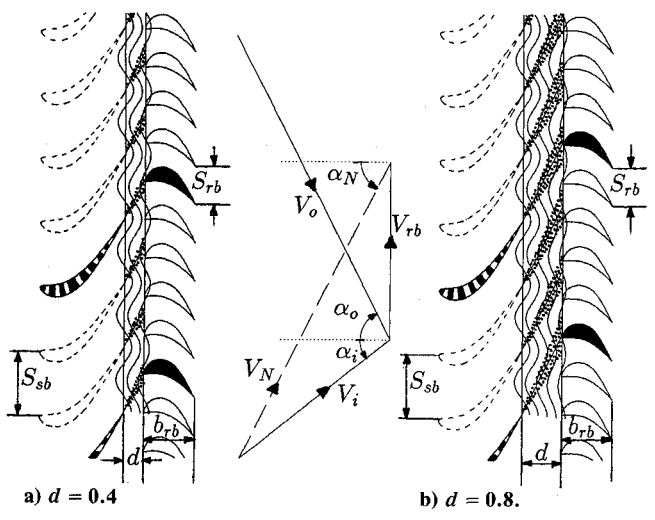

Fig. 1 Effect of stator-rotor gap d on the rotor excitation. The velocity diagrams, upstream stators, and downstream rotors (flow from left to right), and their steady-flow velocity distributions, are identical.

Previous investigations on wake propagation have been published.[1-11] Some experimental results for the combined interaction, and comparisons with theoretical analyses for isolated wake and for isolated potential-flow disturbances as affected by R and d have also been published.[12] In previous investigations,[7-11] the two-dimensional effect of the combination of the viscous wake and of the potential-flow from upstream stators were modeled as incoming flow disturbances into the computational flowfield of the downstream rotors. The resulting unsteady flows in the rotor fields were computed, using the wake and potential-flow models as unsteady inlet-boundary conditions. The effects of two-dimensional vortex shedding (which result in much higher harmonics of much lower amplitude in the forcing functions) were neglected, and infinitely rigid blades without cooling were assumed. New explanations of the effects of the two disturbances were published.[11] For typical stator-rotor gaps ($d \approx 0.30$) and for small values of R ($R < 1.5$) the wake disturbances dominate the unsteadiness onto the downstream cascade, whereas the potential-flow disturbance from the upstream cascade decays before it affects the downstream cascade significantly. For large values of R ($R > 2.5$) the wake disturbance is dwarfed by the potential-flow disturbance, which dominates the unsteadiness onto the downstream cascade. For intermediate values of R ($R \approx 2$), both disturbances influence the unsteady flowfields and result in complex patterns of unsteady pressure regions influencing the forcing functions and stress levels acting on the cascades. The mechanisms of propagation of these disturbances into the rotor flowfields were investigated[10,11] in various rotor cascades of low, intermediate and high aerodynamic loading (tangential-lift coefficients of 0.8, 1.0, and 1.2).

Several Euler and Navier-Stokes calculations of unsteady cascade flow have been published in the literature. The series of papers by Rai[13-16] illustrate that these methods can predict the average unsteady loads acting on the cascades in stator-rotor interactions. An equally important conclusion from Rai's work is that to accurately predict the phases of the unsteady loads, one needs to model accurately both the stator-to-rotor-pitch ratio R and the axial gap between the cascades d. Good modeling of R with Rai's program and other similar programs currently can only be achieved at the expense of considerable CPU time, and this is not feasible for design studies. The importance of d to predict the relative phase of the wake and potential-flow effects (and the resultant phases of the unsteady loads) is illustrated by the relative locations of the disturbances in Fig. 1. Rai has published comparisons of experiments obtained with $R = 28/22 = 1.27273$ with two-dimensional and three-dimensional computations performed with $R = 1$[13-15] and with two-dimensional computations performed with $R = 4/3 = 1.33333$.[16] Rai's work indicates that accurate modeling of R is important to accurately predict the phase of the unsteady loads. This last conclusion is evident if one considers the limiting cases of $R = 1$ (wake disturbances dominate the unsteadiness) and $R = 3$, 4, and 6 (potential interaction disturbances dominate the unsteadiness).[7,9,11]

In our investigations (past and the present one) we used Giles'[17] computer program UNSFLO to compute the flowfields and forces. Initially UNSFLO was an Euler solver for the two-dimensional, unsteady, compressible, inviscid flow around rotor blades. Although later versions of the program can compute viscous stator-rotor flows, we have concentrated on identifying the propagation of the disturbances in the core of the flow using the inviscid version of the program. This program was chosen because it can handle arbitrary values of

R with reasonable CPU and storage requirements, due to a novel "tilting" of the time domain. The accuracy of the computations has already been checked by comparing results of calculations using UNSFLO with the results of numerous steady and unsteady flow cases of known theoretical and experimental output.[7,8,17-20]

Turbomachinery designers have the option of varying, among others, the stator-to-rotor-pitch ratio R and the axial gap between blade rows d. These two parameters can be used to manipulate the magnitude and phase of the unsteady forcing functions (and hence the unsteady stresses) acting on the blades. Our previous investigations[9,11] have already studied the influence of the stator-to-rotor-pitch ratio R. The number of stator and rotor blades are harder to change in the later stages of design. The axial gap between blade rows is somewhat easier to change (although changing this will also change engine length and weight). The purpose of this article is to illustrate and to give some insight on how one may influence (and in some cases minimize) the unsteady flows, unsteady forcing functions, and unsteady stresses by varying the stator-rotor gap. Although in the following we have assumed an upstream stator influencing a downstream rotor, the conclusions can also be used for an upstream rotor influencing a downstream stator.

Rotor-Inlet Boundary

The two disturbances (viscous wake and potential flow) from the stator have been modeled as inputs to the computational rotor-inlet boundary. This simplification provides accurate computational results only if one is extremely careful to specify the correct boundary conditions to the problem. Details of the following derivations have been published elsewhere.[7,8,11,17] The following equations have been included here for clarity and completeness, because they are essential to understanding the model of the rotor-inlet boundary and the following results and discussion.

The velocity disturbance due to the wake is characterized by the maximum amplitude of the velocity defect D, expressed as a fraction of the undisturbed velocity, and by the "width" W of the velocity defect. Most velocity wakes observed in experimental data have velocity profiles that resemble Gaussian distributions. For the wake model we assumed that the velocity defect is a Gaussian distribution with characteristic width expressed as a fraction of the pitch of the blade cascade that generates the wake; in the stator frame the flow vectors in the wake are parallel to the undisturbed flow (a velocity deficit with no angle variation), the static pressure is constant across the wake, and the total enthalpy is constant across the wake. Those assumptions are modeled by

$$u_{iw,q} = \left[1 - D \cdot \exp\frac{1}{2}\left(\frac{\tan(\alpha_n)x - y}{S_{sb}W_q}\right)^2\right] c_n \cos(\alpha_n)$$
$$v_{iw,q} = \left[1 - D \cdot \exp\frac{1}{2}\left(\frac{\tan(\alpha_n)x - y}{S_{sb}W_q}\right)^2\right] c_n \sin(\alpha_n) \quad (3)$$

The stator-rotor gap between blade rows in modern engines is between 0.2 and 0.5 of the axial chords. Narrower gaps result in shorter engines but increase the unsteadiness between the blade rows. Experimental wake data for isolated airfoils, for fan or compressor cascades, and for turbines have been published.[8] The data points in Fig. 2 show turbine wake data.[5,6,21-30]

Typically the suction side of the wakes has larger width than the pressure side. The solid lines represent the values of D and W that were used in this investigation. They were chosen so that they represent the same loss of momentum (4.74%) due to wake at the rotor-inlet boundary, and they are shown in Table 1. A common width has been used for both sides of the wake. (The different widths of the suction and pressure sides have a secondary effect on the unsteadiness propagation mechanisms

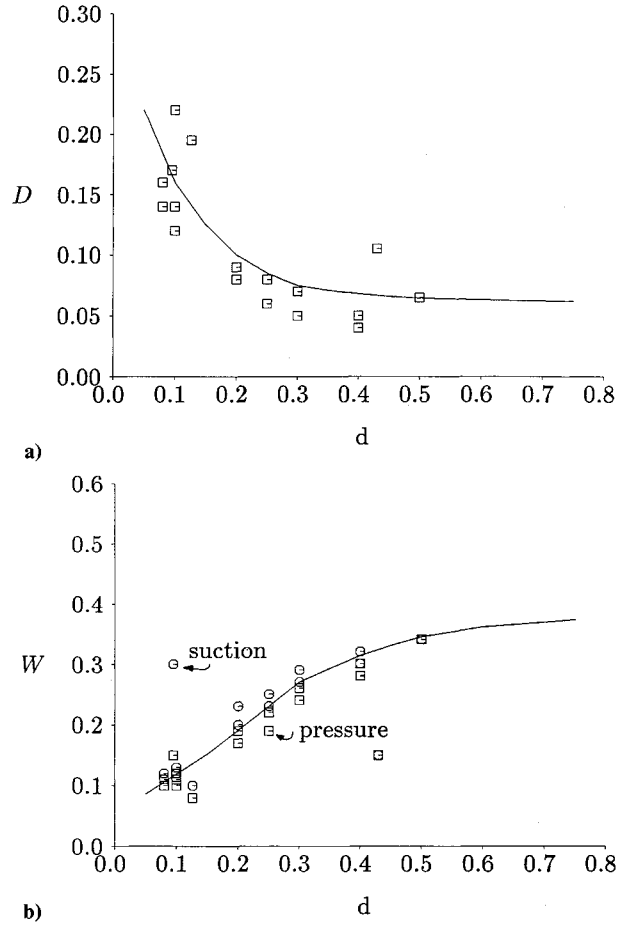

Fig. 2 Experimental turbine-wake data as a function of nondimensional distance downstream from the trailing edge: a) amplitudes D and b) full widths W.

downstream.) In the following, this wake model will be input at the computational rotor-inlet boundary. As shown by Table 1 and Fig. 2, as d increases the amplitude of the wake will decrease and the width of the wake will increase, so that at higher axial gaps the wakes incoming at the computational inviscid rotor-inlet boundary will be thicker.

The model for the potential-flow disturbance is developed by observing experimentally measured and computed static pressure fields of various turbine-blade cascades. Across the line of the trailing edges there is a variation of static pressure with maxima at (or very near) the trailing edges, and minima at (or very near) the middle of the passage. The exact location and shape of the pressure variation depend on the geometric shape of the passage. It is nearly sinusoidal for cascades of various geometries and tangential-lift coefficients, and the amplitude of the pressure disturbance decays very fast with distance downstream. Numerous examples of this static pressure variation have been reviewed in the experimental data of Refs. 7 and 8. Measured cascade data, such as those shown in Fig. 6 of Ref. 31, Fig. 4 of Ref. 32, Fig. 7 of Ref. 33, and Fig. 6 of Ref. 34, show the near-sinusoidal shape and the rapid decay of the potential-flow disturbance. The sinusoidal model is a good representation for many cascade geometries and for high and low tangential-lift coefficients (0.8 to 1.2).[10]

The potential-flow model (in the stator frame) is derived as a two-dimensional, linear, isentropic, irrotational perturbation to uniform flow (modeled by the following nonlinear Eq. 4, taken from page 198 of Ref. 35).

$$(u^2 - a^2)\frac{\partial u}{\partial x} + (v^2 - a^2)\frac{\partial v}{\partial y} + uv\left(\frac{\partial u}{\partial y} + \frac{\partial v}{\partial x}\right) = 0 \quad (4)$$

Table 1 Wake amplitudes D and widths W as a function of stator-rotor gap d

d	D	W
0.05	0.2200	0.0862
0.10	0.1600	0.1185
0.15	0.1250	0.1518
0.20	0.1000	0.1912
0.25	0.0860	0.2266
0.30	0.0750	0.2700
0.35	0.0700	0.2991
0.40	0.0680	0.3134
0.45	0.0645	0.3442
0.60	0.0630	0.3604
0.75	0.0620	0.3726

The velocity-potential relationship is defined by

$$\frac{\partial \Phi}{\partial x} \equiv u \qquad \frac{\partial \Phi}{\partial y} \equiv v \tag{5}$$

For subsonic flows one expects that the potential-flow disturbance from the upstream cascade is periodic (one period per stator pitch) in the y (circumferential or tangential) direction and that it decays exponentially in the x (axial) direction. Thus the general solution of Eq. (4) is of the form

$$\Phi(x,y) = B \cdot \exp\left[j \frac{2\pi}{S_{sb}} y + \xi x \right] \tag{6}$$

where $2\pi/S_{sb}$ dictates the periodicity of the potential Φ. Substituting these (with the negative root of ξ to make the potential disturbance decay downstream) in Eq. (4), solving for Φ and then for the velocity disturbances, we derive

$$\delta v_\phi = -\Delta v_\phi \cdot \exp\left[-\frac{2\pi}{S_{sb}} \frac{\sqrt{1-M^2}}{1-M_x^2} (x - x_{te}) \right] \cdot \sin[2\pi(\epsilon + \Delta\epsilon)] \tag{7}$$

$$\delta u_\phi = -\tan(\alpha_{ip})\delta v - \frac{\sqrt{1-M^2}}{1-M_x^2} \Delta v_\phi \cdot \exp\left[-\frac{2\pi}{S_{sb}} \frac{\sqrt{1-M^2}}{1-M_x^2} (x - x_{te}) \right] \cdot \cos[2\pi(\epsilon + \Delta\epsilon)]$$

where M is given by $M = \sqrt{M_x^2 + M_y^2}$, M_x and M_y are the axial and circumferential Mach numbers in the stator frame, and the phases ϵ and $\Delta\epsilon$ at any location are given by

$$\epsilon = \frac{y - \tan(\alpha_{ip})x}{S_{sb}} \tag{8}$$

$$\Delta\epsilon = \frac{1}{2\pi} \tan^{-1}\left[\frac{\tan(\alpha_n)}{\sqrt{1-M^2}} \right] + \frac{[\tan(\alpha_{ip}) - \tan(\alpha_n)]x_{te}}{S_{sb}}$$

$\Delta\epsilon$ is a phase-shifting constant that locates the maximum amplitude in the pressure disturbance due to the potential-flowfield at the stator trailing edges. Δv_ϕ is the maximum perturbation in circumferential velocity v at the inlet boundary. The velocity perturbations are functions of the axial distance from the inlet boundary. The $\tan(\alpha_{ip})$ is the direction of propagation of the potential field given by:

$$\tan(\alpha_{ip}) = -\frac{M_x M_y}{1 - M_x^2} \tag{9}$$

Equations (7) are coupled with the conditions of no variation in entropy and total enthalpy to give a sinusoidal pressure perturbation Δp of the form:

$$\Delta p = \Delta p_\phi \cos\left\{ 2\pi(\epsilon + \Delta\epsilon) - \tan^{-1}\left[\frac{\tan(\alpha_n)}{\sqrt{1-M^2}} \right] \right\}$$

$$\Delta p_\phi = \frac{pcM\Delta v_\phi}{\sqrt{1-M_x^2}} \tag{10}$$

The following unsteady-flow figures show the resulting shape of Δp in the rotor frame, with a maximum at the stator trailing edges and a minimum between the stator trailing edges. Experimental and computational data reviewed in Ref. 7 indicate that across the line of the trailing edges Δv_ϕ is typically between 4 and 4.5% of the average pressure. The corresponding values of Δv_ϕ for values of V_{rb} typical of modern engines are between 4.52 and 5.31% of c_n. In the computations presented in this paper we used $\Delta v_\phi = 0.04$.

The combined potential flow and wake disturbance from the upstream stator at the rotor-inlet boundary is found by adding the values of the two disturbances. These are input at the computational rotor-inlet boundary via a coordinate transformation for V_{rb}.

Disturbance Propagation

The potential-flow and wake disturbance models propagate in the rotor passages via different mechanisms.[11] These mechanisms are the same for a variety of geometries corresponding to different blade-loading and flow conditions.[10] For large and small values of R there is no possibility of arranging the two mechanisms to counteract each other because one of them dominates the flow. In the remainder of this paper we will concentrate at intermediate values of $R(\approx 2)$, where both disturbances are important, and we will show, by varying the axial gap, how they may be arranged so that they reinforce or counteract each other.

Potential-Flow Disturbance

As the potential-flow disturbance from the stator extends into the rotor cascade, large portions of it enter the passages when the direction of propagation of the potential is aimed near the center of the rotor passage. The potential-flowfield of the stator is cut by the advancing potential flowfield of the rotor. After it is cut, it moves downstream as a potential-flow disturbance in the rotor-relative frame [modeled here with Eq. (10)]. The frequency (with respect to the rotor) and the decay rate of the stator potential-flow disturbance in the rotor cascade are affected by the value of R. Once the potential-flow disturbance is in the rotor passage, its exact location is affected by the geometry and aerodynamic characteristics of the rotor.

Wake Disturbance

A sample unsteady flowfield generated by isolated wake interaction (no potential flow interaction, to show the effects of the wake only) is shown in Fig. 3. It shows the cut wake centerline as thick dashed entropy contours in a rotor passage, superimposed on unsteady-flow vectors and on unsteady-pressure contours (with respect to the average flow) at one time instant. The stator-wake centerlines are first bent by the potential-flowfield of the advancing rotor. As the leading edge in the rotor stagnation region interacts with the lower-momentum fluid in the wake, recirculating-flow patterns are established in the stagnation region of the leading edge of the rotor. These recirculating flow patterns are generated as the wake is being cut; once generated they result in a counterclockwise rotating unsteady-flow pattern downstream of the wake centerline, and a clockwise rotating unsteady-flow pattern upstream of the wake centerline. The wakes are cut by the passing rotor into individual segments that are acting in each passage. After the stator wake is cut to produce a segment of a wake in the rotor passage, the two ends of the wake segment travel at the local speeds: the portion attached to the pressure side moves downstream into the passage much slower than the portion attached to the suction side, because the local flow velocities are higher on the suction side of the cascade. At the same time lower-momentum fluid moves from the wake end near the pressure side to the wake end near the suction side. The last two phenomena cause a thinner wake on the pressure side, a thicker wake on the suction side, and a counterclockwise rotation of the centerline of the wake as it moves through the passage.

Figure 3 shows the cut wake centerline as thick dashed entropy contours in a rotor passage, superimposed on unsteady-flow vectors marking the counter rotating recirculating-flow patterns and superimposed on unsteady pressure contours (with respect to the average flow). The recirculating flows result in regions of increased and decreased unsteady pressure upstream and downstream of the wake centerline, respectively. The negative unsteady pressure regions are marked with thinner double-line contours, to be distinguished from the positive unsteady pressure regions, which are marked with thinner single-line contours. As the recirculating-flow patterns move downstream into the rotor cascade, the wake is sheared, distorted, and enlarged, whereas the amplitude of the unsteady pressure maximum or minimum is decreased and its region of influence increased.

Combined Potential and Wake Disturbance

The corresponding unsteady pressure maxima and minima due to the combined disturbance are the combined effects of the two disturbances just described. The disturbance-propagation mechanisms and explanations of the relative phases of the two disturbances are confirmed by the results of this and past studies. The value of R has a significant effect on which type of disturbance dominates the unsteady flowfield, as already explained in the Introduction.

Forcing Functions

In the following we will examine the forces acting on typical rotor blades from these two disturbances. The dimensional forces per unit length of blade span (such as F_x in the x direction) are related to the nondimensional forces (F_x') by

$$F_x' \equiv \frac{F_x/z}{\rho b_{rb} c_0^2} \tag{11}$$

(The moment M_z' is taken about the leading edge, and it is divided by b_{rb}^2.)

Results

Using the preceding explanations of the mechanisms of generation of unsteady pressure regions due to the wake and the potential from the upstream stator, we can identify (and with insight predict) the regions of influence of the wake and the potential-flow disturbance in the rotor and the resulting shape of the unsteady rotor forcing functions.

Results have been obtained for an intermediately-loaded cascade [incompressible tangential-loading coefficient $C_L = 2S_{rb}\cos^2\alpha_o(\tan\alpha_i - \tan\alpha_o)/b_{rb} = 1.0$] designed with a prescribed-surface-curvature-distribution method.[19] Its design characteristics are shown in Table 2 and its steady-flow performance is shown in Fig. 4.

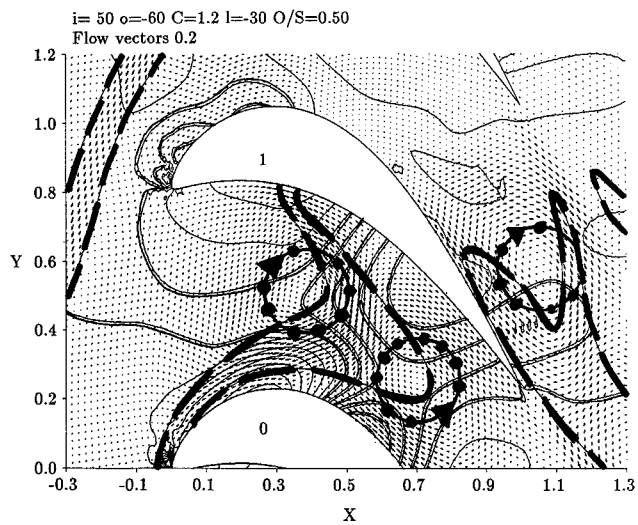

Fig. 3 Unsteady-flow vectors from wakes, illustrating regions of increased and decreased pressure upstream and downstream of the wake centerline (from Ref. 10).

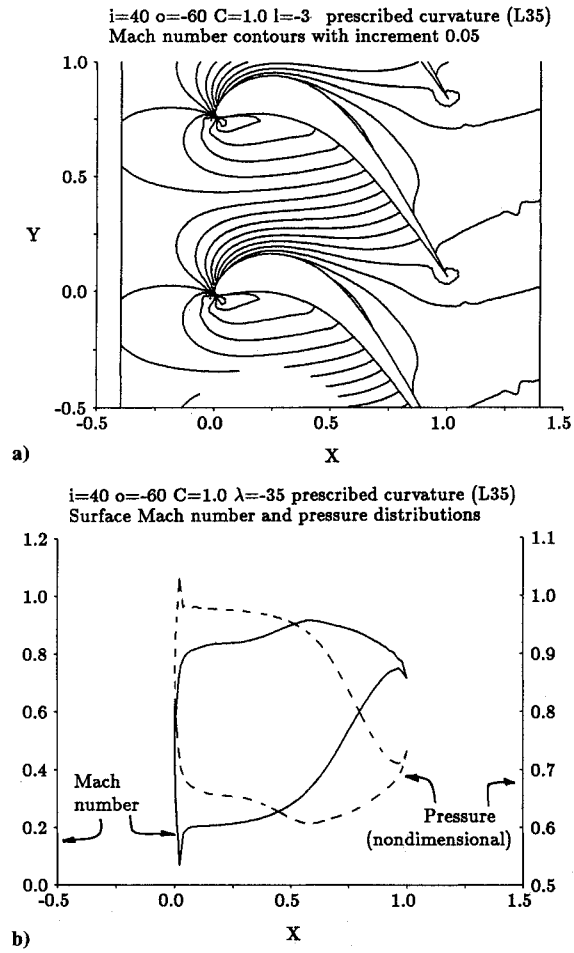

Fig. 4 Steady-flow performance of the sample cascade: a) nondimensional pressure contours of increment 0.02 and b) surface nondimensional pressure and Mach number distributions.

The wake and potential-flow disturbances from the upstream stator have been studied on the sample rotor cascade moving past a stator that has double the pitch of the rotor ($R = 2$). In production engines designers would normally try to choose unequal integers for all blade rows, and R would not be an integer. This value of R has been chosen on purpose for three reasons. First, it is close to the value of R of many turbine stages in production engines. Second, it is in the region where both disturbances are important to the rotor flow, where one has the option of varying the axial gap to arrange the disturbances so that they counteract each other, as shown in the following. Third, $R = 2$ provides a symmetry that facilitates the discussion. Consider three consecutive rotor passages A, B, and C at the same time instant. The flow is repeated every other passage, so that in passages A and C the flow is identical. Because $R = 2$, the flow in passage B is identical to the flow in passages A and B half a period later (or earlier). (Because of the novel tilting of the time domain the program can compute the flowfields for [approximately] $1.5 < R < 2.5$ with the same CPU time.) Results similar to those that follow for $R = 2$ could have been obtained for any other noninteger value of R where both wake and potential disturbances influence the flow.

Figure 5 shows the rotor unsteady pressure contours (thin contours, instantaneous minus average pressure) from the combined disturbances of wake and potential for stator-to-rotor axial gaps $d = 0.30$, 0.50, and 0.75 of the rotor-axial chord, respectively. The regions of positive values of unsteady pressure contours (pressure increased above the average) are dotted; the regions of negative unsteady pressure contain con-

Table 2 Sample cascade[a]

Inlet flow angle α_i, deg	40.00
Outlet flow angle $\alpha_o(<0)$, deg	60.00
Stagger angle (<0), deg	35.00
Loading coefficient C_L	1.00
Cascade solidity S_{rb}/b_{rb}	0.7779
Inlet Mach number	0.405
Outlet Mach number	0.800
Steady-flow x-force $F'_{x,\text{av}}$	0.1179
Steady-flow y-force $F'_{y,\text{av}}$	0.1179
Steady-flow z moment $T'_{z,\text{av}}$	0.1050
Nozzle angle α_n, deg	70.94
V_{rb} for α_n	0.6300
$\tilde{\omega}$ for $R=2$ [see Eq. (2)]	8.2021

[a]Corresponding reduced frequencies can be evaluated using Eq. (2).

tours only. The unsteady pressure contours are superimposed on thicker entropy contours. The figure shows the rotor-relative flow only, for $-0.30<x<1.40$, with the inlet boundary (modeling the stator cascade) moving toward the negative y direction as time increases. For $d=0.30$ the stator trailing edges are at the far left side of the figure (at $x=-0.30$). For $d=0.50$ and 0.75 the stator trailing edge is further upstream (at $x=-0.50$ and -0.75, respectively) than the portions of the field shown in the figure. The centerlines of the wakes could be shown with unsteady vorticity contours, which would be in pairs of negative and positive unsteady vorticity contours, upstream and downstream of the wake centerlines, respectively. To make the figure a little simpler, a single entropy contour is shown to mark the centerline of the wakes.

The origin (zero) of the nondimensional period of the unsteadiness in each case corresponds to the nondimensional time $t=y/S_{sb}=0$. This is the y location at which the centerline of a stator velocity wake touches the leading edge of a rotor blade (numbered blade 0 in the unsteady flow figures). At the same time the next stator wake is touching the leading edge of blade 2. The end of the period $t=y/S_{sb}=1.0$ corresponds to the velocity wake from the next stator blade touching the leading edge of the same rotor blade. Because $R=2$, the same figures show in the immediately above or below passage the flow half a period later (so that the flow at two instants during the period can be seen in each portion of the figure). The flow for $t=y/S_{sb}=0.00$ and for $[t=y/S_{sb}=0.50]$ is shown on the left. The flow for $t=y/S_{sb}=0.33$ and for $[t=y/S_{sb}=0.83]$ is shown in the middle. The flow for $t=y/S_{sb}=0.67$ and for $[t=y/S_{sb}=0.17]$ is shown on the right. The blade numbers in square brackets correspond to flow conditions at times in square brackets. The period of the unsteadiness is one full stator-cascade pitch. The forcing functions for one stator pitch for the three stator-rotor gaps are shown in Fig. 6.

Discussion

Figures similar to Fig. 5 showing the unsteady pressure contours due to the isolated potential-flow disturbance, those due to the isolated wake disturbance, and those due to the combined disturbance for $d=0.30$ for many different cascades and nozzle angles and for different values of R have been included in Refs. 10 and 11. Studying these figures enables one to identify the regions of increased and decreased unsteady pressure due to each type of interaction and to identify the effect of each interaction on the unsteady flowfield. The wake causes regions of positive unsteady pressure upstream of the wake centerlines and regions of negative unsteady pressure downstream of the wake centerlines. The potential-flow disturbances propagate as regions of positive and negative unsteady pressure in the downstream cascades.

The incoming-wake widths, illustrated by the width of the incoming entropy contours in Fig. 5, become thicker with increasing stator-rotor gap because thicker wakes of smaller amplitude have been input for the larger axial gaps, according to Table 1. The figures show the cutting and shearing of the wake by the rotor. Cascades with higher tangential-lift coefficient C_L have higher suction-surface and lower pressure-surface velocities. The centerlines of the cut wakes attached to the suction and pressure sides of the passages, respectively, travel at the local flow velocities downstream. Therefore the wakes are sheared more in cascades with higher values of C_L, when they enter from lower α_n, and when they are wider (larger d).

The effect of the potential-flowfield of the stator on the potential-flowfield of the rotor can be seen by the existence of the unsteady pressure lines at the rotor-inlet boundaries ($x=-0.30$) of all unsteady-flow figures and at all times. The figures show the positive unsteady pressure corresponding to the (modeled) trailing edges of the stators, the negative unsteady pressure between the trailing edges of the stators, and the rapid decay of the potential-flow disturbance downstream of the stator trailing edge. The effect of the stator potential-flowfield at the rotor-inlet boundary ($x=-0.30$) is smaller for larger stator-rotor gaps d. The weaker potential-flowfield

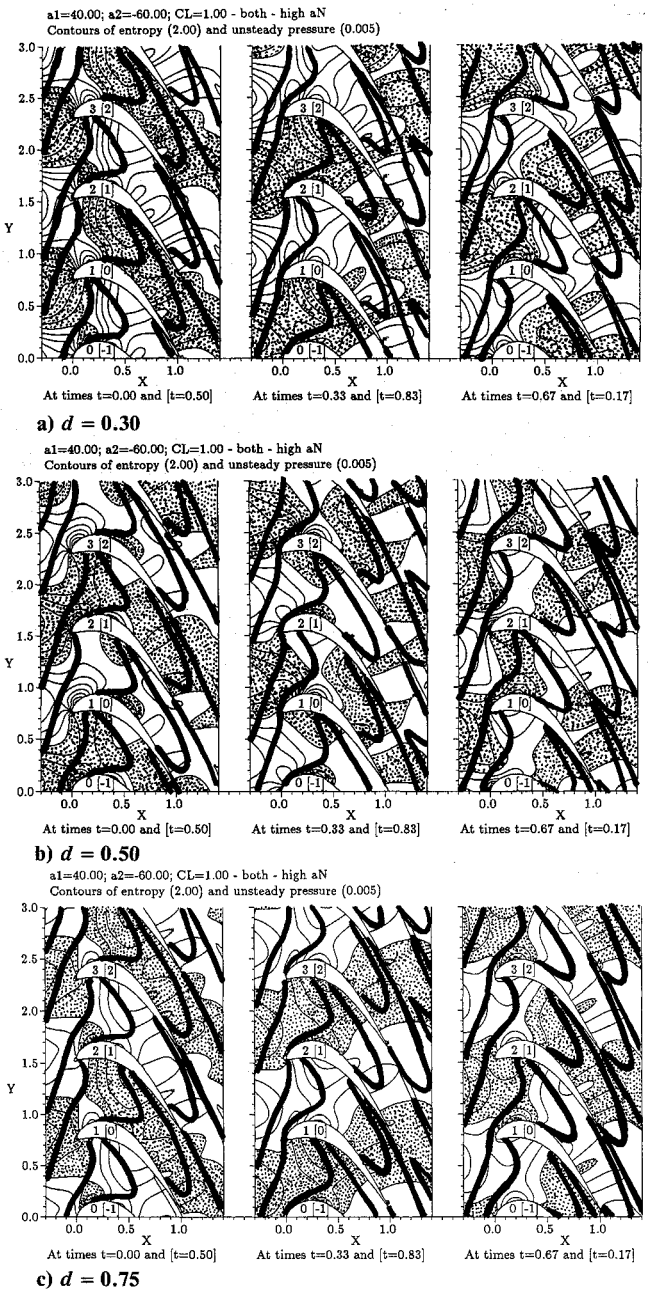

Fig. 5 Propagation of unsteady flowfields. Unsteady pressure contours of increment 0.005 superimposed on entropy contours of increment 2.0.

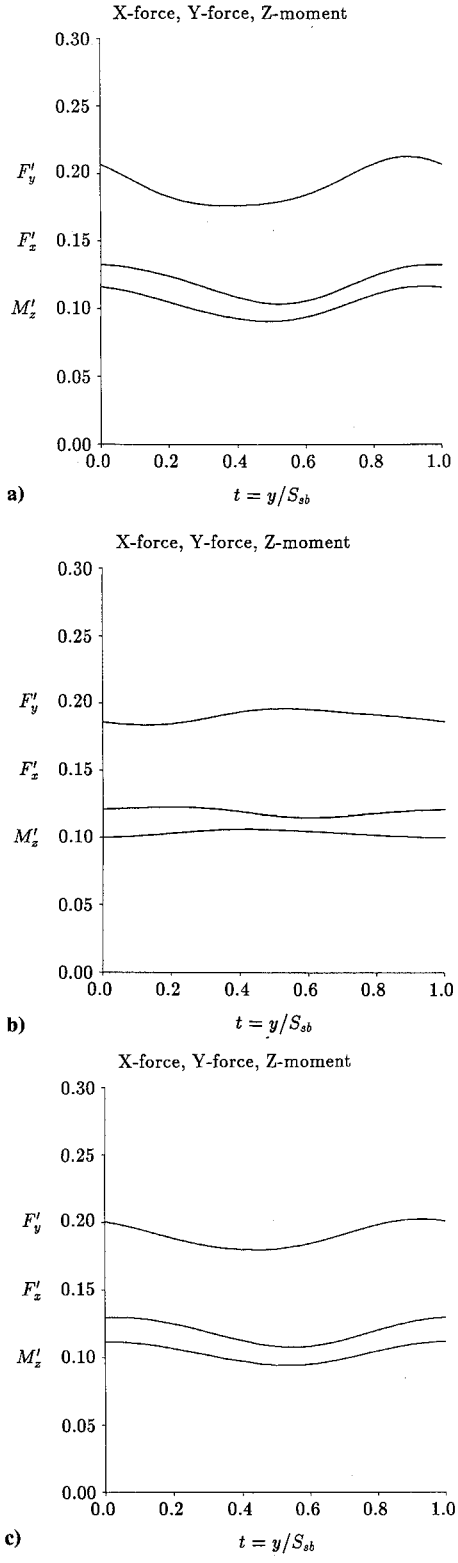

Fig. 6 Forcing functions on the rotor: a) $d = 0.30$, b) $d = 0.50$, and c) $d = 0.75$.

of the rotor blades propagates upstream, distorts, and eventually cuts the stronger potential-flowfield of the stator. The portion cut in the passage propagates downstream as a potential-flow disturbance (in this study according to [Eqs. (10)], transformed in the rotor-relative frame, and superimposed on the rotor flowfield). The effect of the potential-flowfield of the rotor upstream can also be seen by the distortion (bending) of the wake centerlines near the leading edge of the rotors.

At corresponding times in Fig. 5 the wakes are at the same locations (except they are thicker at larger stator-rotor gaps). The unsteady pressure maxima and minima generated by the stator potential-flow disturbance are at different locations, reflecting that they started from different trailing edge locations (originated at different values of x). The regions of positive and negative unsteady pressures from the wake and the potential are superimposed. For example at the top of Fig. 5 at time $t = 0.0$ and near $(x, y) = (0.4, 0.5)$, the negative unsteady pressure from the potential is superimposed on the negative unsteady pressure from the wake, resulting in large negative values of pressure. One passage upstream, near $(x, y) = (0.5, 1.2)$, the positive unsteady pressure from the potential is superimposed on the positive unsteady pressure from the wake, resulting in large positive values of pressure. The combination of "in phase" unsteady pressures around blade 0 results in substantial variations in F'_y. As d increases, the location of maxima and minima due to the stator potential change and eventually become "out of phase" with those due to the wake. This occurs (at corresponding times and places to that just documented) in the center of Fig. 5 ($d = 0.50$). At time $t = 0.0$ and near $(x, y) = (0.4, 0.5)$, the positive unsteady pressure from the stator potential is superimposed on the negative unsteady pressure from the wake, resulting in small (local) positive values of pressure. One passage upstream, near $(x, y) = (0.5, 1.2)$, the negative unsteady pressure from the stator potential is superimposed on the positive unsteady pressure from the wake, resulting in small (local) positive values of pressure. The combination of unsteady pressures around blade 0 results in very small variations in F'_y. The effects of the potential and the wake become "in phase" again at $d \approx 0.75$, shown at the bottom of Fig. 5. For these larger values of stator-rotor gap the stator potential-flow disturbance onto the rotor is substantially reduced due to its decay downstream. The influence of the wake is also reduced (due to spreading of the wake downstream) but to a much lesser extent. The unsteady part of the forcing functions at $d = 0.50$ is a little smaller than that at $d = 0.75$, and is the smallest of those at stator-rotor gaps $0.2 < d < 0.75$. The last statement has been verified by obtaining the unsteady flowfields and forcing functions at the corresponding stator-rotor gaps in increments of 0.05.

The results presented here are representative results of many studies in cascades with subsonic inflow and outflow, of various tangential-loading coefficients and velocity distributions, and of various values of R and d. In all cases where the two disturbances from the wake and the potential flow are comparable in magnitude ($1.5 < R < 2.5$), they can be arranged to counteract each other at suitable values of d. The unsteady forces do not decrease monotonically as d increases. Their magnitude depends on the relative location of the two disturbances at each value of d.

The results indicate that by varying R and d one may find geometries in which (for most of the period) the influence of wake and stator potential-flow disturbances counteract each other to minimize the unsteady forces. This occurs to large parts of the period in the center of Fig. 5, where $d = 0.5$. In contrast, one can also find geometries in which (for most of the period) the influence of wake and stator potential reinforce each other to maximize the unsteady forces. This occurs to large parts of the period at the top and bottom of Fig. 5 where $d = 0.3$ and 0.75, respectively.

Conclusions

The unsteady forces on two-dimensional gas-turbine rotors, resulting from variations of the average flowfield due to potential-flow and viscous-wake disturbances from upstream blade rows, are computed using a compressible, two-dimensional, inviscid rotor/stator-disturbance program. The viscous wake and the potential-flow disturbances from the upstream stator are modeled at the rotor-inlet boundary. The mechanisms of generation of unsteady forces on the rotor blades are

reviewed. The results used in this paper to facilitate the discussion have been compared with the results from numerous other cascades of a variety of loading distributions and geometries. The reasoning presented in this paper is confirmed by all cases we have studied to date. The mechanisms of propagation of the potential and wake disturbances for the sample cases examined here are those discussed in previous studies.

We conclude the following:

1) For values of stator-to-rotor-pitch ratio where both wake and potential-flow disturbances are of comparable magnitude and neither one dominates the other ($1.5 < R < 2.5$), one can vary the axial gap between blade rows to find where the unsteady pressures, unsteady forces, and unsteady stresses acting on the blades are minimized. The unsteady effects do not always decrease monotonically with increasing stator-rotor gap.

2) The mechanisms and locations of generation of unsteady pressure distributions due to the upstream blade row potential-flow and wake disturbances are different. Designers could use the preceding arguments (and the understanding of where the local pressure maxima and minima from the two disturbances are located) to influence the shape of the unsteady forcing functions and minimize the magnitude of the unsteadiness. This can be done by varying the stator-to-rotor-pitch ratio and the axial gap between blade rows.

3) Analyses of this type will enable turbomachinery designers to predict and understand the magnitude and phase of the forcing functions acting on turbomachinery stages. Understanding the effect of various geometric design modifications on the shape of the unsteady forcing functions will enable designers to reduce the unsteady forces and stresses acting on turbomachinery blades.

Acknowledgments

The author thanks M. B. Giles and Rolls Royce plc. for their permission to use UNSFLO in this investigation, and Christine Korakianitis for patiently marking the dotted regions in Fig. 5.

References

[1]Meyer, R. X., "The Effect of Wakes on the Transient Pressure and Velocity Distributions in Turbomachines," *Transactions of the American Society of Mechanical Engineers,* Vol. 80, 1958, pp. 1544–1552.

[2]Lefcort, M. D., "An Investigation of Unsteady Blade Forces in Turbomachines," *Transactions of the ASME, Journal of Engineering for Power,* Vol. 87A, 1965, pp. 345–354.

[3]Smith, L. H., "Wake Dispersion in Turbomachines," *Transactions of the ASME, Journal of Basic Engineering,* Vol. 88, Sept. 1966, pp. 688–690.

[4]Kerrebrock, J. L., and Mikolajczak, A. A., "Intra-Stator Transport of Rotor Wakes and Its Effect on Compressor Performance," *Transactions of the ASME, Journal of Engineering for Power,* Oct. 1970, pp. 359–371; also ASME Paper 70-GT-39, 1970.

[5]Hodson, H. P., "An Inviscid Blade-to-Blade Prediction of a Wake-Generated Unsteady Flow," *Transactions of the ASME, Journal of Engineering for Gas Turbines and Power,* Vol. 107, April 1985, pp. 337–344; also ASME Paper 84-GT-43, 1984.

[6]Hodson, H. P., "Measurements of Wake-Generated Unsteadiness in the Rotor Passages of Axial Flow Turbines," *Transactions of the ASME, Journal of Engineering for Gas Turbines and Power,* Vol. 107, April 1985, pp. 467–476; also ASME Paper 84-GT-189, 1984.

[7]Korakianitis, T., "A Design Method for the Prediction of Unsteady Forces on Subsonic, Axial Gas-Turbine Blades," Sc.D. Dissertation, Massachusetts Inst. of Technology, Cambridge, MA, Sept. 1987.

[8]Korakianitis, T., "On the Prediction of Unsteady Forces on Gas Turbine Blades: Part 1: Description of the Approach," *Transactions of the ASME, Journal of Turbomachinery,* Vol. 114, No. 1, 1992, pp. 114–122.

[9]Korakianitis, T., "On the Prediction of Unsteady Forces on Gas Turbine Blades: Part 2: Analysis of the Results," *Transactions of the ASME, Journal of Turbomachinery,* Vol. 114, No. 1, 1992, pp. 123–131.

[10]Korakianitis, T., "Blade-Loading Effects on the Propagation of Unsteady Flows and on Forcing Functions in Axial-Turbine Cascades," *Journal de Physique III,* Vol. 2, No. 4, 1992, pp. 507–525.

[11]Korakianitis, T., "On the Propagation of Viscous Wakes and Potential-Flow in Axial-Turbine Cascades," *Transactions of the ASME, Journal of Turbomachinery* Vol. 115, No. 1, 1993, pp. 118–127; also ASME Paper 91-GT-373, 1991.

[12]Gallus, H. E., Grollius, H., and Lambertz, J., "The Influence of Blade Number Ratio and Blade Row Spacing on Axial-Flow Compressor Stator Blade Dynamic Load and Stage Sound Pressure Level," *Transactions of the ASME, Journal of Engineering for Power,* Vol. 104, July 1982, pp. 633–641; also ASME Paper 81-GT-165, 1981.

[13]Rai, M. M., "Navier-Stokes Simulations of Rotor/Stator Interaction using Patched and Overlaid Grids," *Journal of Propulsion and Power,* Vol. 3, No. 5, 1987, pp. 387–396; also AIAA Paper 85-1519.

[14]Rai, M. M., "Three-Dimensional Navier-Stokes Simulations of Turbine Rotor-Stator Interaction; Part I—Methodology," *Journal of Propulsion and Power,* Vol. 5, No. 3, 1989, pp. 305–311; also AIAA Paper 87-2058.

[15]Rai, M. M., "Three-Dimensional Navier-Stokes Simulations of Turbine Rotor-Stator Interaction; Part II—Results," *Journal of Propulsion and Power,* Vol. 5, No. 3, 1989, pp. 312–319; also AIAA Paper 87-2058.

[16]Rai, M. M., and Madavan, N. K., "Multi-Airfoil Navier-Stokes Simulations of Turbine Rotor-Stator Interaction," *Transactions of the ASME, Journal of Turbomachinery,* Vol. 112, July 1990, pp. 377–384; also AIAA Paper 88-0361, 1988.

[17]Giles, M. B., "Calculation of Unsteady Wake/Rotor Interactions," *Journal of Propulsion and Power,* Vol. 4, No. 4, 1988; also AIAA Paper 87-0006, 1987.

[18]Giles, M. B., and Haimes, R., "Validation of a Numerical Method for Unsteady Flow Calculations," *Transactions of the ASME, Journal of Turbomachinery,* Vol. 115, No. 1, 1993, pp. 110–117; also ASME Paper 91-GT-271, 1991.

[19]Korakianitis, T., "Prescribed-Curvature Distribution Airfoils for the Preliminary Geometric Design of Axial Turbomachinery Cascades," *Transactions of the ASME, Journal of Turbomachinery,* Vol. 115, No. 2, 1993, pp. 325–333; also ASME Paper 92-GT-366, June 1992.

[20]Korakianitis T., and Papagiannidis, P., "Surface-Curvature-Distribution Effects on Turbine-Cascade Performance," *Transactions of the ASME, Journal of Turbomachinery,* Vol. 115, No. 2, 1993, pp. 334–341; also ASME Paper 92-GT-84, June 1992.

[21]Dring, R. P., Josyln, H. D., Hardin, L. W., and Wagner, J. H., "Turbine Rotor-Stator Interaction," *Transactions of the ASME, Journal of Engineering for Power,* Vol. 104, No. 4, 1992, pp. 729–742; also ASME Paper 82-GT-3, 1982.

[22]Hodson, H. P., "Unsteady Boundary-Layers on Axial-Flow Turbine Rotor Blades," Ph.D. Dissertation, Univ. of Cambridge, UK, Feb. 1983.

[23]Chen, S., "Application of the Rotating Water Table to Nozzle Wake Excitation in Low Pressure Turbines," ASME Paper 85-IGT-45, 1985.

[24]Moore, J., and Adhye, R. Y., "Secondary Flows and Losses Downstream of a Turbine Cascade," *Transactions of the ASME, Journal of Engineering for Gas Turbines and Power,* Vol. 107, No. 4, 1985, pp. 961–968; also ASME Paper 85-GT-64, 1985.

[25]Hubensteiner, M, "Einflub der Schaufelprofilform auf die instationaren Schaufelkrafter eines mittleren Turbinengitters (Influence of the Blade-Figure on the Unsteady Blade-Forces of a Middle Turbine Stage)," *VDI Berichte,* 1986, pp. 209–232.

[26]Binder, A., and Romey, R., "Secondary Flow Effects and Mixing of the Wake Behind a Turbine Stator," *Transactions of the ASME, Journal of Engineering for Power,* Vol. 105, No. 1, 1983, pp. 40–46; also ASME Paper 82-GT-46, 1982.

[27]Binder, A., Forster, W., Kruse, H., and Rogge, H., "An Experimental Investigation into the Effects of Wakes on the Unsteady Turbine Rotor Flow," *Transactions of the ASME, Journal of Engineering for Gas Turbines and Power,* Vol. 107, No. 2, 1985, pp. 458–466; also ASME Paper 84-GT-178, 1984.

[28]Binder, A., "Turbulence Production due to Secondary Vortex Cutting in a Turbine Rotor," *Transactions of the ASME, Journal of Engineering for Gas Turbines and Power,* Vol. 107, No. 4, 1985, pp. 1039–1046; also ASME Paper 85-GT-193, 1985.

[29]Binder, A., Forster, W., Mach, K., and Rogge, H., "Unsteady Flow Interaction Caused by Stator Secondary Vortices in a Turbine Rotor," *Transactions of the ASME, Journal of Turbomachinery,* Vol. 109, No. 2, 1987, pp. 251–257; also ASME Paper 86-GT-302, 1986.

[30]Wittig, S. Dullenkopf, G., Schulz, A., and Hestermann, R.,

"Laser-Doppler Studies of the Wake-Effected Flow Field in a Turbine Cascade" *Transactions of the ASME, Journal of Turbomachinery,* Vol. 109, No. 2, 1987, pp. 170–176; also ASME Paper 86-GT-160, 1986.

[31]Sonoda, T., "Experimental Investigation on a Spatial Development of Streamwise Vortices in a Turbine Inlet Guide Vane Cascade," ASME Paper 85-GT-20, 1985.

[32]Yamamoto, A., and Yanagi, R., "Production and Development of Secondary Flows and Losses Within a Three-Dimensional Turbine," ASME Paper 85-GT-217, 1985.

[32]Boletis, E., and Sieverding, C. H., "Experimental Study of the Flow Field Behind an Annular Turbine Nozzle Guide Vane with and Without Downstream Rotor," ASME Paper 84-GT-15, 1984.

[34]Sieverding, C. H., Van Hove, W., and Boletis, E., "Experimental Study of the Tree-Dimensional Flow Field in an Annular Turbine Nozzle Guidevane," *Transactions of the ASME, Journal of Engineering for Gas Turbines and Power,* Vol. 106, No. 2, 1984, pp. 437–448; also ASME Paper 83-GT-120, 1983.

[35]Liepmann, H. W., and Roshko, A., *Elements of Gasdynamics,* Wiley, New York, 1957, p. 198.